Investigating an organ-targeting platform based on hydroxyapatite nanoparticles using a novel in situ method of radioactive [125]Iodine labeling

Nenad Ignjatović[1], Sanja Vranješ Djurić[2], Žarko Mitić[3], Drina Janković[2], Dragan Uskoković[1*]

[1]*Centre for Fine Particles Processing and Nanotechnologies, Institute of Technical Sciences of the Serbian Academy of Science and Arts, Knez Mihailova 35/4, 11000 Belgrade, Serbia,*

[2]*Laboratory for radioisotopes, Vinča Institute of Nuclear Sciences, University of Belgrade, PO Box 522, 11001 Belgrade, Serbia,*

[3]*Faculty of Medicine, Department of Pharmacy, University of Niš, Bulevar dr Zorana Đinđića 81, 18000 Niš, Serbia*

Abstract

In this study, we have investigated the synthesis of nanoparticles of hydroxyapatite (HAp) and hydroxyapatite coated with chitosan (HAp/Ch) and the chitosan-poly-D,L-lactide-co-glycolide polymer blend (HAp/Ch-PLGA) as an organ-targeting system. We have examined and defined the final destination, as well as the dynamics and the pathways of the synthesized particles following intravenous administration *in vivo*.

The XRD, ZP, FT-IR and SEM analyses have confirmed that the hydroxyapatite nano particles with d50=72 nm are coated with polymers. Radioactive 125-Iodine (^{125}I), a low energy gamma emitter, was used to develop a novel *in situ* method for the radiolabeling of particles and investigation of their biodistribution. ^{125}I–labeled particles exhibited high stability in saline and serum over the second day, which justified their use in the following *in vivo* studies.

----

* Author for correspondence (dragan.uskokovic@itn.sanu.ac.rs).

The biodistribution of ^{125}I-labeled particles after intravenous injection in rats differed significantly: HAp particles mostly targeted the liver, HAp/Ch the spleen and the liver, while HAp/Ch-PLGA targeted the lungs. Twenty-four hours post injection, HAp particles were excreted completely, while both [125]I- HAp/Ch and ^{125}I-HAp/Ch-PLGA were retained in the body for a prolonged period of time with more than 20% of radioactivity still found in different organs.

1. Introduction

Nanoparticles based on hydroxyapatite (HAp) have many useful physicochemical and biological properties, such as an easy preparation and modification, as well as biocompatibility, which make them suitable for transport and unloading of various pharmaceuticals [1-3]. Nanoparticulate systems based on polymers or polymer-coated inorganic particles are a challenge for many research groups involved in designing materials for the replacement of tissues and other specific medical applications [4]. Hydroxyapatite nanoparticles coated with bioresorbable polymers have been successfully used as carriers of antibiotics, vitamins and stem cells in bone tissue engineering [5, 6]. Over the past few decades, different nanoparticulate platforms for targeted and temporal delivery have been studied for possible use in therapeutic applications [7]. Some researchers highlight the benefits of nanosystems ensuring local and controlled delivery of a drug compared to conventional systems, particularly in the regeneration of bone tissue [8]. There are various strategies of drug targeting, from passive to active targeting, dependening on the potential clinical application and the structure and properties of the system [9]. Interactions in the microenvironment of biomaterials and tissues are of a particular interest and present a challenge in regenerative nanomaterials engineering [10]. A study on targeted drug delivery can also be focused on the cell and its proteins [11]. The phenomena that influence the success of targeting and controlled operation or regenerative or therapeutic nanosystems are

numerous and complex: size, shape, surface charge, functional groups of nanoparticles, electrical double-layer formation, zeta potential, isoelectric point of solid–liquid interface; receptor–ligand binding interactions of nano-bio interface etc [12].

Chitosan is one of many natural biopolymers with a wide range of potential applications in regenerative medicine. Structurally, chitosan is a copolymer composed of randomly distributed β-(1→4)-linked D-glucosamine (GlcNH$_2$) and N-acetyl-D-glucosamine (GlcNAc), obtained by the deacetylation of chitin, though the deacetylation is almost never complete [13]. Chitosan is considered one of the most valuable polymers for biomedical and pharmaceutical applications due to its biodegradability, biocompatibility, antimicrobial, non-toxicity and anti-tumor properties [14, 15]. The use of chitosan has proved to be reasonable in complex systems of targeted drug delivery in neurology [16]. Some researchers have focused on the unification of the desirable properties of HAp and chitosan and obtaining a hybrid system in order to improve the functionality of potential applications of such systems [17, 18]. Hybrid systems based on HAp and chitosan have shown an extremely rapid formation of a new bone and mineralization of a reconstructed bone defect [19]. In order to modify the properties of chitosan in the systems for controlled and targeted action, it was combined with poly-D,L-lactide-co-glycolide (PLGA) and; the research results indicate the validity of the applied concept [20, 21].

In this study, we have examined the possibility of obtaining an organ-targeting carrier based on hydroxyapatite nanoparticles. The dependence of surface properties of small particles based on hydroxyapatite is studied: zeta potential, morphology, crystallinity/amorphousness and chemical groups, on their transport/pathways in the biological environment after intravenous administration. The subject of the study are nanoparticles of hydroxyapatite, uncoated and coated with chitosan and the chitosan-poly(DL-lactide-co-glycolide) blend. Radioactive iodine ^{125}I was used for radiolabeling of newly synthesized particles in order to study their *in vivo* biological behavior.

2. Experimental

2.1 Synthesis of materials

Aqueous calcium nitrate ($Ca(NO_3)_2$) solution (150 ml; 26.6wt%) was added to the solution of ammonium phosphate (($NH_4)_3PO_4$) (7 ml H_3PO_4 + 165 ml NH_4OH + 228 ml H_2O) at 50°C over the period of 60 minutes, while stirring at the rate of 100 rpm. The solution was then subjected to a heat treatment for 60 minutes at 100°C [22, 23]. The obtained gel was subjected to frozen vacuum drying at -10 to -60°C, under pressures between 0.37 and 0.1 mbar over the periods between one and four hours (Christ Alpha 1-2/LD Plus). The obtained product was hydroxyapatite powder (HAp).

Chitosan (Ch), of a low molecular weight (Aldrich, deacetylation>75%) dissolved in acetic acid (1 wt.%) was mixed with the HAp gel in the 4:6 mass ratio while stirring with a magnetic stirrer at 400 rpm. Distilled water was added drop-wise to the mixture of chitosan and HAp gel, while stirring at 21,000 rpm (Ultra-Turrax T25, IKA, Germany). The obtained mixture of chitosan and the HAp gel was slowly poured into glutaraldehyde solution (Grade I, 25% in H_2O) at the speed of 21,000 rpm for one hour. The resulting mixture was then centrifuged at 5000 rpm and 5 °C for one hour (Hettich Universal 320R). The obtained powder was subjected to frozen vacuum drying at temperatures from −10 to −60 °C, under pressures between 0.37 and 0.1 mbar over the periods between one and six hours. The obtained product was the powder composed of chitosan-coated HAp particles (HAp/Ch).

PLGA (50:50, Sigma, USA) and chitosan dissolved in acetone and acetic acid were mixed with the HAp gel in the mass ratio of 2:2:6. Water solution of poloxamer 188 (polyethylenepolypropylene glycol, 0.1 vol.%) was added drop-wise to the mixture of chitosan, PLGA and HAp gel, while stirring at 21,000 rpm. The obtained mixture of chitosan, PLGA and the HAp gel was slowly poured into glutaraldehyde solution (Grade I, 25% in H_2O) at the speed of 21,000 rpm for one hour. The obtained mixture was then centrifuged at 500 rpm and 5 °C for one hour, and the obtained powder was subjected to frozen vacuum drying at −10 to −60 °C, and

pressures from 0.37 mbar to 0.1 mbar for one to eight hours. The obtained product was the powder composed of HAp particles coated with chitosan-poly(D,L)-lactide-co-glycolide (HAp/Ch-PLGA).

2.2 Characterization of the products

X-Ray diffraction (XRD) was performed on a Philips PW-1050 diffractometer with Ni-filtered $Cu_{K\alpha}$ radiation. The scanning step was 0.02°. Electrokinetic parameters of the suspensions of synthesized particles were analyzed using a Zeta-Sizer Nano (Malvern Instruments Ltd.) in distilled water and pH 6.5. Infrared spectroscopy (FTIR) was done on a BOMEM MB-100 spectrometer (Hartmann & Braun, Canada), using the KBr technique in the spectral range from 400 to 4000 cm^{-1}. The spectral resolution was 2 cm^{-1}. The field-emission scanning electron microscopy (FE-SEM) measurements were performed on a MIRA 3 MXU (High resolution SEM, Tescan) microscope. The particle size distribution (PSD) was measured on 10 mg/ml of powders dispersed in water using a Mastersizer 2000 (Malvern Instruments Ltd.) and a *HydroS* dispersion unit for liquid dispersants.

2.3 Labeling of HAp (HAp/Ch and HAp/Ch-PLGA) with [125]I (*in situ* labeling)

All radioactive materials were handled according to approved protocols at the Laboratory for radioisotopes, Vinca Institute of Nuclear Sciences. $Na^{125}I$ ($E\gamma = 35$ keV, $T1/2 = 60$ days, carrier-free) was purchased from Izotop (Budapest, Hungary) as a high concentration solution in 0.1M NaOH. HAp was radiolabeled with ^{125}I by a modification of the chloramine T method [24] during their preparation and before the addition of chitosan or chitosan-poly(D,L)-lactide-co-glycolide. 185 MBq of Na ^{125}I was added to 10 mL of HAp suspension. The reaction was started by the addition of 0.2 mL of chloramine T (*N*-chloro-*p*-toluenesulfonamide (CAT), sodium salt, trihydrate; Merck, Darmstadt, Germany) solution (50 mg/mL, molar ratio HAp:CAT=4:1) in 0.05M a phosphate buffer (pH 7.5). The mixture was tightly capped in the reaction flask and

stirred for one hour at room temperature. The reaction was stopped by adding 0.3mL of sodium thiosulfate (100 mg/mL). The mixture was then centrifuged (at 10,000 rpm for 10 min) to precipitate ^{125}I-labeled HAp. After the removal of the supernatant, the radiolabeled HAp obtained as a precipitate was subjected to further washings (for three times) to separate any unbound ^{125}I. The ^{125}I-activity of the supernatant and pellet were measured in a gamma counter (CompuGama 1282 LKB, Finland) using the manufacturer's settings for ^{125}I. The labeling yield of the ^{125}I-HAp was calculated as (radioactivity in pellet/total radioactivity before washes) x100%. Afterwards^{125}I- labeled HAp was coated with chitosan or chitosan-poly(D,L)-lactide-co-glycolide, according to the procedure described in 2.1

2.4 *In vitro* stability studies

In vitro stability of ^{125}I- labeled HAp, HAp/Ch and HAp/Ch-PLGA was studied to determine any released ^{125}I- activity from the radiolabeled particles in biological fluids during eight days. After ^{125}I-labeling suspensions of all three types of ^{125}I-labeled nanoparticles (37 MBq) were centrifuged (at 10,000 rpm for 10 min). The supernatant was withdrawn and after addition of 3 mL either saline (0.9% NaCl, pH=7.3) or human serum (National Blood Transfusion Institute, Belgrade, Serbia) samples were incubated by shaking at 37°C. At eight time points after the labeling (1-8 days), samples were centrifuged. Due to the risk of the withdrawal of ^{125}I- labeled particles, the supernatant was not removed completely. Instead, an aliquot of 0.1 mL was carefully withdrawn from the supernatant and the radioactivity was measured separately in an aliquot and the remaining sample (pellet with labeled particles and 2.9 mL of supernatant). The acquired radioactivity in the pellet was calculated as the difference between ~~follows:~~ the activity of the remainder and the activity of the supernatant (0.1 mL supernatant x 2.9). The *in vitro* stability of the labeled particles in biological fluids is expressed as a percentage of the particle-associated radioactivity (radioactivity in the pellet) in relation to the total radioactivity in the sample. The experiments were done in triplicate.

2.5 Biodistribution studies

The entire animal study conformed to ethical guidelines and the rules for animal care proposed by the Serbian Laboratory Animal Science Association (SLASA) and also complied with the Directive 2010/63/EU of the European Parliament and of the Council. Biodistribution studies of [125]I- labeled HAp were carried out in groups of five normal male Wistar rats (one month old, 100–150 g in weight). An amount of 0.1 mL of the suspension of radiolabeled particles in saline contained 0.1 mg of [125]I- labeled -HAp, -HAp/Ch or -HAp/Ch-PLGA (activity 2 MBq) was injected through the tail vein of each animal.

The groups of rats were sacrificed at various time intervals (10min, 30min, 2h and 24h) post injection (p.i.) and blood and the tissues, including the heart, lungs, liver, spleen, kidney, stomach, intestine, muscles, femur and thyroid gland were harvested, weighed, and counted for 1 min in a gamma counter. Standards were prepared and measured along with the samples, whereas the total counts injected per animal were calculated by the difference between the original syringe counts and the remaining syringe counts after injection. The uptake of the radiolabeled particles in each tissue sample was calculated as a fraction of the injected dose and was expressed as percentage injected dose per gram of tissue or organ (%ID/g).

3.   Results

3.1 X-Ray diffraction (XRD)

Figure 1 shows the diffractograms of HAp/Ch- PLGA, HAp/Ch, HAp and pure Ch and PLGA. The absence of the peaks in the diffractogram of PLGA indicates the amorphous nature of the polymer. Ch is defined with the diffractogram with two clearly marked peaks in the positions 10.2° and 19.8°. The most intense peaks of HAp are on 31.8° (2 1 1), 32.2° (1 1 2), 32.9° (3 0 0), 25.9° (0 0 2) and 49.5° (2 1 3). In accordance with the literature [25] and our previous studies [23], the HAp diffractogram obtained this way indicates poorly a crystalline form. The mean

crystallite size (D) of the HAp powders calculated from the half-width (β1/2) of the XRD reflection of the (002) plane (2θ=25.9°) using the Scherrer equation was 11.8 nm.

Figure 1.

3.2 Zeta potential (ZP) measurements

HAp particles have the value of -7.9±0.8, HAp/Ch +18.3±1.9 and HAp/Ch-PLGA +3.0±0.28. All values were measured in aqueous suspensions of particles at pH=6.5 and t=20^{0}C.

3.3 FTIR spectroscopy analysis

The IR spectra of HAp, Ch, PLGA, HAp/Ch and HAp/Ch-PLGA samples are shown in Fig. 2. and the following characteristic IR bands were identified on wavenumbers: ν(OH) 3600–3000 cm^{-1} (HAp, PLGA, Ch; intensive, wide band), ν(NH$_2$) 3500–3400 cm^{-1} (Chi; two bands, medium intensity, overlapped with a wide band of ν(OH)), ν(CH) 2900 cm^{-1} (HAp, PLGA, Ch; medium intensity), ν(C=O) 1755 cm^{-1} (PLGA; strong intensity), ν(C=O) 1655 cm^{-1} (amide I band, Ch; strong intensity), δ(HOH) approx. 1640 cm^{-1} (HAp, PLGA, Ch; weak to medium intensity), δ(NH) 1580 cm^{-1} (amide II band, Ch; medium intensity), δ_{sy}(CH) 1380 and δ_{as}(CH) 1450 cm^{-1} (HAp, PLGA, Ch; weak to medium intensity), δ (OH) 1420 cm^{-1} (HAp, PLGA, Ch; medium intensity), ν(C–O) 1250–1050 cm^{-1} (PLGA, Ch; strong intensity), ν(C–N) 1320 cm^{-1} (amide III band, Ch; medium intensity), ν(P=O) 1100 cm^{-1} (HAp; strong intensity), ν(P–O) 1030 cm^{-1} (HAp; strong intensity overlapped with a band ν(P=O)), γ(CH) and γ(OH) 1000–700 cm^{-1} (HAp, PLGA, Ch; weak intensity) [26]. In the area of approx. 860–875 cm^{-1}, carbonate band appears from the carbonate substitution for hydroxyl and phosphate groups in hydroxyapatite [27].

Figure 2.

3.4 Particle size distribution (PSD)

The particle size distribution (PSD) of the synthesized HAp, HAp/Ch and HAp/Ch- PLGA are shown in Fig. 3. The average mass diameter d(0.5) or d50 which indicates that 50% of the particles are less than the specified value and 50% greater, amounts for HAp d50=70 nm, HAp /Ch d50=130 nm and HAp/Ch-PLGA d50=163 nm. The synthesized HAp particles have a uniform distribution, while the system HAp/Ch and HAp/Ch-PLGA shows the appearance of particle agglomerates of about 700 nm in diameter.

Figure 3.

3.5 Field-emission scanning electron microscopy (FE-SEM)

The FE-SEM images of HAp, HAp/Ch and HAp/Ch-PLGA are shown in Fig. 4. By coating the particles of HAp with Ch, powders with spherical particles were obtained (Fig. 4b). The coating of HAp with a polymer blend Ch-PLGA also leads to the formation of particles with a spherical morphology (Fig. 4c). The results of the particle size distribution of HAp/Ch-PLGA (Fig. 3) with the possibility of forming agglomerates were confirmed with the existence of adhesion between individual particles (Fig. 4c). Quantitatively, the frequency of the formation of the HAp/Ch material agglomerate is not significant because only 10% of the fraction is greater than 820 nm (d90=820 nm).

Figure 4.

3.6 Labeling of HAp, HAp/Ch and HAp/Ch-PLGA with ^{125}I

In order to radiolabel particles with a specific radionuclide, two approaches can be used: the encapsulation of the radionuclide in the nanocarrier during the synthesis; and, after the synthesis of particles, direct incorporation of the radionuclide onto the particle surface or onto a chelator that is already attached to the particle surface. The labeling of particles after the preparation usually requires modification, such as amination of HAp for effective radioiodination [28]. In

this study, all three types of HAp particles were radiolabeled with ^{125}I during preparation of HAp before the addition of chitosan or chitosan-poly(D,L)-lactide-co-glycolide. Labeling without any modification was achieved by adding the oxidizing agent chloramines T *in situ* during the formation of HAp. This method resulted in the reproducible high labeling yield (78.2%) of ^{125}I-labeled HAp. Studies on the effect of the concentration of the oxidizing agent on the radiolabeling yield showed that the yield was significantly higher when the concentration of chloramines T was increased in the reaction mixture up to 10 mg, while it decreased significantly when chloramines T concentrations decreased above this. The radiolabeling yield was only 12.5% when 2.5 mg of CAT was used (molar ratio HAp:CAT=1:1). The iodination of unmodified HAp after the preparation and during the preparation without the oxidizing agent chloramines T resulted in a complete absence of labeling. The variation of the pH of the reaction mixture showed that the optimum pH for radiolabeling was ~7.5-8, which is advantageous, as it is close to the physiological pH. The radiolabeling yield increased gradually with the incubation time and reached the optimum value after 60 min of incubation at room temperature. No differences in labeling yields were found between the three types of HAp after the addition of chitosan or chitosan-poly(D,L)-lactide-co-glycolide since the labeling step was completed during the formation of HAp.

3.7 *In vitro* stability studies

The *in vitro* stability of the labeled particles expressed as a percentage of the particle-associated radioactivity demonstrated the satisfactory stability of ^{125}I-HAp both in saline and human serum (Fig. 5.). Radioactivity of the supernatant derived from the ^{125}I released from ^{125}I-labeled particles ~~NPs~~. The *in vitro* stability studies in saline showed that 47±2% of ^{125}I remained associated with uncoated HAp particles, while 71±3% and 83±2% remained associated with HAp coated chitosan and chitosan-poly(D,L)-lactide-co-glycolide, respectively, after eight days of incubation. Results of the *in vitro* stability in serum showed a similar trend: uncoated ^{125}I-

HAp particles showed the lowest stability 42±1% after eight days of incubation, while 71±4% of ^{125}I-HAp/Ch and 78±3% of ^{125}I-HAp/Ch-PLGA were stable to deiodination until the eighth day.

Figure 5.

3.8 Biodistribution studies of ^{125}I-labeled HAp, -HAp/Ch and -HAp/Ch-PLGA

The distribution patterns of ^{125}I-HAp, ^{125}I-HAp/Ch and ^{125}I-HAp/Ch-PLGA in different tissues after 10 min, 30 min, 2 h and 24 h of intravenous administration in normal Wistar rats are shown in Fig. 6.

Figure 6.

The applied radiolabeled HAp particles disappeared from the blood-stream relatively quickly and only 0.22 %ID/g of radioactivity remained in the blood 10 min p.i. The coating with polymers prolonged the *in vivo* circulation of particles, resulting in the highest activity of ^{125}I-HAp/Ch in the blood 30 min p.i. (1.36%ID/g). ^{125}I-HAp mainly accumulated in the liver (20.70%ID/g) during the initial time intervals (10 min). HAp/Ch were quickly taken up by the reticuloendothelial system (RES) of liver and spleen where they were almost equally distributed: 11.04%ID/g in the liver and 14.41%ID/g in the spleen. However, almost 80%ID/g of the applied HAp/Ch-PLGA were localized in the lungs, much less in the liver (5.04 %ID/g) and in the spleen (1.88 %ID/g) 10 min after intravenous administration. The accumulated radioactivity immediately started to wash-out from the organs. Both coated ^{125}I- HAp/Ch and ^{125}I-HAp/Ch-PLGA were excreted in the same amount (nearly 70%) through the hepatobiliary tract of the animals, while uncoated HAp was excreted completely in 24 h post application. There was no sign of radioactivity in the thyroid gland and stomach at any time, indicating the *in vivo* stability of all three types of ^{125}I- HAp and the absence of the destruction of the labeled complex. These results are in good correlation with the results of significant *in vitro* stability of all three types of ^{125}I- HAp in the human serum.

4. Discussion

The absence of strong peaks in the diffractogram of PLGA indicates the amorphous nature of this polymer. The existence of two distinct peaks in the diffractogram of chitosan 2θ at 10.2° and 19.7° indicates its high crystallinity, which is consistent with studies of other authors [29]. As it has been shown in our previous study, the diffraction pattern of HAp in Fig. 1 corresponds to poorly crystalline non-stoichiometric HAp [23]. The diffractograms of HAp/Ch and HAp/Ch-PLGA samples (Fig. 1) indicate that the resulting material is made of HAp and Ch. In both diffractograms clear peaks originating from HAp and Ch are observed. According to the XRD studies performed on HAp/Ch systems by other authors, the peaks group at 2θ about 20° could indicate the intramolecular interaction between HAp and Ch and the formation of a hydrogen bond [17]. The less prominent characteristic peak of chitosan in the HAp/Ch and HAp/Ch-PLGA composite than in the pure Ch on 2θ at 19.7° may not be merely a consequence of the reduction of the share of Ch in the composite but also indicates the possibility that the crystallinity of Ch may be reduced during the process of the composite synthesis [30].

It is known from literature data that HAp particles have negative values of the zeta potential [31, 32]. The coating of HAp with Ch, which has a positive zeta potential, is expected to result in a change of the surface properties and the reversal of the negative zeta potential to positive (~~Fig. 2~~). When in a slightly acidic environment, chitosan enters the electrostatic interaction with the negatively charged environment due to the protonation of the free $-NH_2$ groups [33]. The positive electric charge of chitosan and the potential of creating hydrogen bonds indicates its good adhesion properties in a biological environment [34] which may be of interest during the testing of these materials *in vivo*. The values of the zeta potential of PLGA, which depends on a number of factors (end groups of PLGA, surface charge density, type of stabilizing agent utilized during syntheis etc.), are all in the range of negative values. It is expected that HAp coated with Ch-PLGA has a lower value of the zeta potential than HAp coated only with Ch. The resultant

trends are consistent with other studies focused on the analysis of the zeta potential of the Ch-PLGA systems of different compositions [35, 36].

The IR spectrum of the HAp/Ch composites sample is shown in Fig. 2. The IR spectrum is characterized by absorption bands arising from HAp and Ch, determined by analogy with the IR spectra of uncoated HAp and the same Ch standard samples (as illustrated in Fig. 2). The analysis of the FTIR spectrum in Fig. 2 reveals significant differences compared to the spectra of single-component materials. The sharp bands at 2923 and 2862 cm^{-1} are assigned to ν(CH) of the polysaccharide chitosan [37] and IR bands with maxima at 1087, 1033, 601 and 564 cm^{-1} arise from the phosphate groups of HAp [38]. The formation of homogeneous Ch blends with HAp and PLGA is a result of strong interactions of hydrogen bonds between the functional groups of the blend components in which amino and amide groups present in Ch take part [39]. The analysis of the FTIR spectra of the blends enables us to identify these interactions. The broadening of the strong IR band at approx. 1087 cm^{-1}, corresponding to the PO_4^{3-} ions of HAp shows the presence of polysaccharide chitosan and its interaction with phosphate groups [40]. It implies that the hydrogen bonding may be formed between the phosphate groups and N–H of the Ch [41]. The peaks at 1655 cm^{-1}, 1588 cm^{-1} and 1315 cm^{-1} are due to the amide I, amide II and amide III bands of polysaccharide chitosan. The band at 1655 cm^{-1} decreased and the band at 1588 increased in Ch after the coating of HAp, indicating the interaction of the amide on the chitosan and OH groups on HAp. Considerably greater changes are observed in the spectrum of the HAp/Ch-PLGA composites sample. The IR spectrum of the sample of hydroxyapatite coated with the polymer blend of chitosan-poly(lactide-co-glycolide) (HAp/Ch-PLGA) is shown in Fig. 2. The IR spectrum contains the already mentioned absorption bands arising from HAp, PLGA, Ch (as illustrated in Fig. 2). The specific IR bands of polysaccharide chitosan were observed at around 3500–3200 cm^{-1} for N–H stretching, at 2980–2880 cm^{-1} for C–H stretching, at 1737 cm^{-1} for C=O stretching, at 1588 cm^{-1} for N–H bending, at 1500–1350 cm^{-1} for C–H bending and approx. 1310cm^{-1} for C–N stretching. A comparison of the FTIR spectra of HAp, PLGA and

HAp/Ch-PLGA shows a specific peak shift due to the interaction of HAp with the polymer blend of Ch-PLGA. The differences in the FTIR spectra, i.e. the shift to lower wavenumbers and the narrowing of the vibration band from 1756 cm^{-1} to 1737 cm^{-1}, which originates from ν(C=O), have been observed. This is probably due to the hydrogen bonding of C=O from PLGA with OH or NH$_2$ from HAp or chitosan, which confirms their mutual interaction and particle formation. In the study of three-phase interactions in nano-hydroxyapatite/konjac glucomannan/chitosan composite amide I, the carbonyl stretching in Ch shifts to lower wavenumbers; this is attributed to the hydrogen bonding between the NH, C=O groups of konjacglucomannan/chitosan and OH from HAp [41]. The most significant differences in the FTIR spectra of HAp/Ch-PLGA compared to HAp/Ch are the increase in the band at 1588 (amide II) and the overlapping of the band at 1655 cm^{-1} (amide I) in the polymer blends of Ch-PLGA after the coating of HAp. This indicates the interaction of the amide on the chitosan and the OH groups on HAp. The appearance of new band, pronounced as a shoulder, at a lower frequency, approx. 3239 cm^{-1}, which originates from the hydrogen bonded OH is due to the interactions between HAp and Ch-PLGA. This is confirmed by the well-modified surface of the Ch-PLGA polymer blends after the coating of HAp. The addition of chitosan also affected the localized bonding structure of the phosphate groups in HAp, as seen from the broadening of the PO$_4^{3-}$ group bands [26]. The 1000–700 cm^{-1} IR range is of special interest for structural investigations of polysaccharides and conformational changes, and both the number and frequencies of the bands in this IR range depend on the conformation of the D-glucopyranose units [42]. It is well known that the D-glucopyranose units exist in six different typical conformations (^{1}C, C$_1$, ^{1}B, B$_1$, ^{3}B and B$_3$) [42, 43]. The similarities of the γ(C–H) range indicate that there is no difference in the conformation of the GlcNH$_2$ and GlcNAc units in the Ch, HAp/Ch and HAp/Ch-PLGA, and they probably exhibit C$_1$ chair conformation (bands approx. 915 and 850 cm^{-1}). As mentioned earlier [44], in β-D-glucans and their derivatives, only one most stable chair conformation C$_1$ (^{4}C$_1$) of pyranose cycles is achieved and their mutual mobility is strongly limited. But in water, at equilibrium,

GlcNAc undergoes a microsecond-timescale exchange between chair puckers ($^4C_1$ and $^1C_4$), which is in good agreement with the NMR measurements and high-resolution crystallographic data for protein-bound GlcNAc ligands, where an appreciable number are not $^4C_1$ conformers [45]. The results from literature [45] challenge the hypothesis that GlcNAc is a perfectly rigid $^4C_1$ chair, as predicted by high-level energy calculations without explicit water, straightforward interpretation of NMR data and non-equilibrium nanosecond-simulations. In the 1000–970 cm^{-1} range, several bands are observed in the IR spectra of chitosan (approx. 1000, 993 and 984 cm^{-1}). The appearance of these components is characteristic of polysaccharides with β-configuration of (1→4) glycosidic bond [46]. The ring deformations and scaffold vibrations for polysaccharide chitosan are observed at 705, 665, 605, 570, and 520 cm^{-1}.

The uniform distribution of HAp particles is obtained (Fig. 3.) with d10=36nm, d50=70 nm and d90=156 nm. After the freeze-drying of the HAp/Ch powder, particles with the distribution of d10=66nm, d50=130 nm and d90=260 nm are obtained (Fig. 3.). It is assumed that the increase in the diameter of the obtained particles is due to the coating of HAp with Ch, but it is to a lesser degree also present in the appearance of the agglomerate, which is in accordance with the FE-SEM analysis (Fig. 4c). HAp/Ch-PLGA powder has a distribution of d10=73nm, d50 =163 nm and d90=820 nm, indicating a trend of the increase in the average diameter of the particles in the sequence d(HAp) → d(HAp/Ch) → d(HAp/Ch-PLGA) and all fractions. HAp particles in all systems have the same diameter, and the increase in the diameter is the consequence of coating HAp with polymer and also of potential agglomeration. Agglomeration is more pronounced in the HAp/Ch-PLGA system, compared to HAp/Ch, which is expected, according to the results of the zeta potential. In accordance with the obtained values of d50, it was possible to presume the average thickness of the coatings: [d50(HAp/Ch)-d50(HAp)]/2~30 nm; [d50(HAp/Ch-PLGA)-d50(HAp)]/2~47 nm.
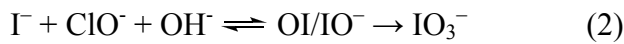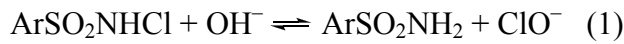
In our previous research, we have demonstrated the possibilities and the mechanism of coating particles and small nano-sized agglomerates of HAp with bioresorbable polymers in the form of spheres [23, 47]. After two-stage emulgation procedure and subsequent processing in a centrifugal field, platet-like HAp is coated with Ch and spherical shapes are obtained (Fig. 4a, b), which is in accordance with XRD, ZP and FT-IR results. A similar morphology is observed in the system HAp/Ch-PLGA (Fig. 4c), except for the slightly larger diameter of the particles, which is also in accordance with the PSD results (Fig. 3.). Subsequent processing in the centrifugal field and the synthesis with a high energy emulsifier leads to obtaining a spherical particle morphology [47].

As part of our ongoing effort to produce HAp vectors for different biomedical purposes, we have herein developed the efficient method for their radiolabeling with the aim of monitoring the biodistribution of the synthesized particles. Due to their small size, it is a challenging task to track and detect particles *in vivo*. The *in vivo* behavior of HAp has not been reported extensively due to the lack of suitable tracking methods. Fluorescent labeling is achieved only for a short term, while qualitative findings and the inductively coupled plasma (ICP) spectrometry method hardly yield precise results due to the degradation of particles [48]. A promising technique for the following distribution of particles in biological systems is the use of radiotracers, due to the high sensitivity, accuracy and precision of radioactivity measurements. The choice of radionuclide depends on a number of characteristics including the type of particles, ease of preparation and the stability of radionuclide-particles conjugate as well as the availability, cost and the decay characteristics of the radionuclides [49]. The *in vivo* biodegradation processes and reversible isotope exchange processes can lead to instability and escape of radionuclides [50]; accordingly, the binding of the radionuclide to a nanoparticle has to be irreversible in order to prevent their release into the immediate environment. Also, the manufacturing process has to be fast and simple in order to decrease the risk of contamination. ^{90}Y and ^{177}Lu are a practical choice for labeling of HAp having in mind that by employing a simple technique HAp can be

radiolabeled with these radionuclides in a very high yield. The key issues concerning the use of ^{90}Y are its physical and chemical characteristics and the biodistribution profile. As a pure β-emitter, ^{90}Y cannot be measured accurately by a standard gamma counter; it can only be detected by "bremsstrahlung", so measurements by a standard gamma counter are not accurate [51, 52]. Also, the *in vivo* release of ^{90}Y and ^{177}Lu from the labeled particles would result in the misinterpretation of biodistribution results, especially in the studies where the same organs are targets both for these radionuclides and the labeled particles and their degradation products. ^{90}Y and ^{177}Lu in their ionic form have a high affinity for bone, while in colloidal form (after the dissociation from the labeled compounds in blood) they would be cleared through the liver [53]. Since most of the labeled particles accumulate in these organs, ^{90}Y and ^{177}Lu are not the ideal radionuclides for labeling of the studied particles.

^{125}I is a readily available radionuclide with a low gamma-ray energy that can be used for tracking and quantifying *in vivo*. The circulating iodide is removed rapidly by both the thyroid gland and the stomach due to sodium iodide symporter (NIS)-mediated active transport. In other tissues, which do not express NIS, the uptake of sodium iodide is significantly lower than in NIS-expressing tissues and decreased over time, paralleling blood-pool clearance and excretion in the urine [54]. Since a misinterpretation of the biodistribution results of ^{125}I-labeled particles is almost impossible due to the biodistribution of particles in NIS non-expressing tissues, ^{125}I seems to be a good choice for the labeling of the investigated particles. Also, the labeling procedure optimized for the labeling of particles with ^{125}I can be used for the labeling with beta emitting radionuclide ^{131}I, ensuring a therapeutic effect. The present study describes for the first time the efficient radiolabeling of HAp with ^{125}I *in situ* in the presence of an oxidant, such as chloramine-T. The radioiodination is probably based on the incorporation of some of the iodine species into the apatite lattice. Chloramine-T, $ArSO_2NClNa$ ($Ar=CH_3C_6H_4$), behaves as an oxidizing agent in both acidic and alkaline media. The nature of active oxidizing species depends on the pH of the medium and the reaction conditions.

$$ArSO_2NHCl + OH^- \rightleftharpoons ArSO_2NH_2 + ClO^- \quad (1)$$

$$I^- + ClO^- + OH^- \rightleftharpoons OI/IO^- \rightarrow IO_3^- \quad\quad (2)$$

$$3HOI = IO_3^- + 2I^- + 3H^+ \quad\quad\quad\quad (3)$$

In alkaline solutions, the predominant species of CAT are $ArSO_2NHCl$ and ClO^- [Eq. (1)]. With a further increase in the alkalinity, the concentration of hypochlorite ions increases [55]. The iodide ion is oxidized by hypochlorite in the basic solution to hypoiodous acid (HOI), which can be deprotonated to hypoiodite (IO^-) according to Eq. (2), and the equilibrium between the two species is established. Hypoiodite can be further oxidized to iodate (IO_3^-), whereas HOI can undergo rapid disproportionation to iodate and iodide (pH > 8) Eq. (3). These anions probably make coordination similar to carbonate anions on phosphate or hydroxide sites in the lattice. Since only small amounts of radioactive iodine were involved in radioiodination, the oxidized iodine species produced in the reaction with chloramine T could not influence crystal growth in HAp and other modifications in the HAp structure. This mechanism is more favorable than the intercalation of solvated/hydrated free iodide ions into molecular crystals of HAp. In aqueous solutions, sodium iodide typically dissociates to completion with the formation of free solvated ions. This method based on labeling without adding chloramine T did not result in the radioiodination of HAp and radiolabeling after the completion of the formation of HAp particles when iodine species could not enter the molecular crystal of HAp. The procedure used in this study allowed simple manipulations for labeling and purification and resulted in a highly efficient labeling yield (78%) of radiolabeled HAp particles. Therefore, the *in vivo* deiodination process was attenuated in two ways: by optimization of the labeling process and by washing of labeled HAp particles after the initial labeling until the most of ^{125}I conjugated to the particles *via* labile physical adsorption had been eluted. Although this reduced the labeling yield, the *in vitro* and *in vivo* deiodination processes were also attenuated.

The *in vitro* stability studies (Fig.5.), have demonstrated that all three types of particles are stable and that they release less than 8 % of ^{125}I from ^{125}I-labeled nanoparticles in saline and

serum until the second day, enabling *in vivo* studies during this period. The higher stability of both coated ^{125}I-labeled-HAp/Ch and -HAp/Ch-PLGA over a week could be assigned to the protective effect of ~~chitosan and~~ polymers on the surface of HAp particles. The coated particles are probably less porous, thereby preventing the diffusion of ^{125}I out and away from the particles. The accumulation of ^{125}I in the thyroid and the stomach was negligible, indicating an *in vivo* stability of the radiolabeled particles.

The physical and chemical properties, including size, charge, and surface chemistry, greatly influence the pharmacokinetics and the tissue distribution of the particles [56]. Unlike small molecules that can diffuse through the capillary wall into the tissue, particles pass through the gaps between the cells of endothelium in certain tissues, such as tumors, liver, spleen or bone marrow [56]. Small HAp particles (~70 nm) easily penetrated through the endothelial wall in the liver (the pore size of liver fenestrae is 100 nm) resulting in the fast initial increase in the activity within this organ but poor retention. Regarding the tumor uptake, small particles behave similarly. They can easily pass through the leaky capillary wall in the tumor but can also be easily pushed out from the tumor into the blood. The results of the biodistribution of liposomes of different sizes have shown similar behavior as HAp particles. Liposomes smaller than 100 nm in size exhibit minimal spleen uptake, whereas an increase in particle size leads to an increase in the rate of spleen uptake [57].

Similarly to other nanomaterials, the *in vivo* pharmacokinetics and *in vivo* biodistribution of HAp particles are closely associated with their surface coatings. Beside the particle size (Fig 3.), the following parameters also significantly affect the *in vivo* particle distribution: zeta potential, the surface groups of coatings (Fig 2.) and the particle shape (Fig 4.). The clearance of ^{125}I-HAp from the systemic circulation is very fast in the first 10 min after the intravenous injection. The coating with chitosan prolonged the circulation half-life of particles, so ~~that~~ an increased concentration of ^{125}I-HAp/Ch in blood (almost seven times) 10 min p.i., as well as an extended circulation time ~~was~~ were revealed. When particles are intravenously administered, serum

proteins also termed "opsonins", bind on the particles which are recognized by the scavenger receptor on the macrophage cell surface and internalized, leading to a significant loss of particles from the circulation [58]. The accumulation of ^{125}I-HAp/Ch mainly in the liver and spleen and a longer retention compared to the uncoated HAp particles are attributed to the endocytosis by macrophages of reticuloendothelial system (RES) of these tissues. A high accumulation of HAp/Ch-PLGA in the lungs indicates that particles were mechanically filtered by the capillary bed of the lungs. Therefore, the high accumulation of HAp/Ch-PLGA in the lungs probably occurred due to the aggregation of particles. Therewith, a small but detectable percentage (>0.1 %) of ^{125}I-HAp/Ch-PLGA was still circulating 24 h after the administration. The different uptakes of ^{125}I-labeled-HAp/Ch and HAp/Ch-PLGA particles by the lungs and liver as well as the retention rate in these organs verify that physicochemical characteristics significantly affect the *in vivo* fate of particles.

5. Conclusion

The XRD, FT-IR and ZP analyses have confirmed that hydroxyapatite (HAp) particles with d50=70 nm are coated with chitosan (HAp/Ch) and the chitosan-poly-D,L-lactide-co-glycolide polymer blend (HAp/Ch-PLGA). The FTIR results of HAp/Ch and HAp/Ch-PLGA composites show the interaction between single components, which confirms strong interactions by hydrogen bonds between the functional groups of the blend components in which, amino and amide groups present in Ch take part. After the coating of HAp with Ch and Ch-PLGA, more round particle shapes were obtained compared to uncoated HAp.

It has been shown that the radiotracer technique with ^{125}I-labeled HAp nanoparticles is a relevant approach to study the biodistribution of novel particles. The labeling method was optimized for ^{125}I-labeling *in situ*, during the synthesis of particles. The *in vitro* studies in saline and human serum have revealed that ^{125}I remains bound to particles for a period sufficient for a further *in vivo* application. HAp/Ch and HAp/Ch-PLGA particles exhibited rather different *in*

vivo behaviors compared to uncoated HAp particles, after they had been intravenously injected. HAp particles mostly targeted liver, HAp/Ch spleen and liver and HAp/Ch-PLGA lungs. Along with the difference in targeting the final destination, the coated nanoparticles show different pharmacokinetics in terms of slower excretion compared to HAp. This study demonstrates that the composition of the coating of HAp nanoparticles determines their biodistribution properties, which has significant implications with regard to their application in controlled drug delivery and targeting.

Acknowledgements

References

[1] Y. Cai, R. Tang, J. Mater. Chem. 18 (2008) 3775-3787.

[2] S.V. Dorozhkin, Acta Biomater. 6 (2010) 715-734.

[3] V. Uskoković, D. Uskoković, J. Biomed. Mater. Res. B 96 (2011) 152–191.

[4] R. Langer, D. Tirrell, Nature 428 (2004) 487-492.

[5] C. Gandhimathi, J. Venugopal, R. Ravichandran, S. Sundarrajan, S. Suganya, S. Ramakrishna, Macromol. Biosci. 13 (2013) 696-706.

[6] R. Ravichandran, J.R. Venugopal, S. Sundarrajan, S. Mukherjee, S. Ramakrishna, Biomaterials 33 (2012) 846–855.

[7] A. Swami, J. Shi, S. Gadde, A. Votruba, N. Kolishetti, O. Farokhzad, Nanoparticles for targeted and temporally controlled drug delivery, in: S. Svenson, R. Prud'homme (Eds.), Multifunctional nanoparticles for drug delivery applications, imaging, targeting, and

delivery. Series: nanostructure science and technology, Springer Science+Business Media, LLC, 2012, pp. 9-31.

[8] W. Gu, C. Wu, J. Chen, Y. Xiao, Int. J. Nanomedicine 8 (2013) 2305-2317.

[9] R. Lehner, X. Wang, S. Marsch, P. Hunziker P, Nanomedicine 9 (2013) 742–757.

[10] J. Rice, M. Martino, L. De Laporte, F. Tortelli, P. Briquez, J. Hubbell, Adv. Healthc. Mater. 2 (2013) 57-71.

[11] M. Martinez, R. Jafari, M. Ignatushchenko, T. Seki, E. Larsson, C. Dan, L. Sreekumar, Y. Cao, P. Nordlund, Science 341 (2013) 84-87.

[12] A. Nel, L. Madler, D. Velegol, T. Xia, E. Hoek, S. Somasundaran, F. Klaessig, V. Castranova, M. Thompson, Nat. Mater. 8 (2009) 543–557.

[13] M. Kumar, React. Funct. Polym. 46 (2000) 1–27.

[14] M. Kumar, R. Muzzarelli, C. Muzzarelli, H. Sashiwa, A. Domb, Chem. Rev. 104 (2004) 6017-6084.

[15] H. Sashiwa, S. Aiba, Prog. Polym. Sci. 29 (2004) 887–908.

[16] J. Kim, W. Choi, Y. Kim, G. Tae, Biomaterials 34 (2013) 1170-1178.

[17] F. Li, Y. Liu, Y. Ding, Q. Xie, Soft Matter, 10 (2014) 2292-2303.

[18] H. Liu, H. Peng, Y. Wu, C. Zhang, Y. Cai, G. Xu, Q. Li, X. Chen, J. Ji, Y. Zhang, H. OuYang, Biomaterials 34 (2013) 4404-4417.

[19] T. Fernández, G. Olave, C. Valencia, S. Arce, J. Quinn, G. Thouas, Q.Z. Chen, Tissue Eng. A. doi:10.1089/ten.TEA.2013.0696

[20] P. Zeng, Y. Xu, C. Zeng, H. Ren, M. Peng, Int. J. Clin. Pharm. 415 (2011) 259–266.

[21] C. Stigliano, S. Aryal, M. deTullio, G. Nicchia, G. Pascazio, M. Svelto, P. Decuzzi, Mol. Pharm. 10 (2013) 3186–3194.

[22] N. Ignjatović, Z, Ajduković, V. Savić, D. Uskoković, J. Biomed. Mater. Res. B 94 (2010) 108–117.

[23] N. Ignjatović, C-Z. Liu, J. Czernuszka, D. Uskoković, Acta Biomater. 3 (2007) 927-935.

[24] W. Hunter, F. Greenwood. Nature 194 (1962) 495-496.

[25] International Center for Diffraction Data, JCPDS file No. 09-432

[26] R. Kumar, K. Prakash, P. Cheang, L. Gower, K. Khor, J. R. Soc. Interface. 5 (2008) 427–439.

[27] J. Barralet, S. Best, W. Bonfield, J. Biomed. Mater. Res. 41 (1998) 79-86.

[28] J. Sun, G. Xie, J. Nanosci. Nanotechnol. 11 (2011) 10996–11000.

[29] L. Qi, Z. Xu, X. Jiang, C. Hu, X. Zou, Carbohydr Res 339 (2004) 2693–2700.

[30] S. Teng, E. Lee, B. Yoon, D. Shin, H. Kim, J. Oh., J. Biomed. Mater. Res. A 88 (2009) 569–580.

[31] J. Knowles, S. Callcut, G. Georgiou, Biomaterials 21 (2000) 1387-1392.

[32] S. Swain, S. Dorozhkin, D. Sarkar, Mater. Sci. Eng. C 32 (2012) 1237-1240.

[33] P. He, S. Davi, L. Illum, Int. J. Pharm. 166 (1998) 75-88.

[34] N. Schipper, S. Olsson, J. Hoogstraate, A. deBoer, K. Varum, P. Artursson, Pharm. Res. 14 (1997) 923-929.

[35] L. Chronopoulou, A. Cutonilli, C. Cametti, M. Dentini, C. Palocci, Colloids. Surf. B Biointerfaces 97 (2012) 117-123.

[36] S. Fischer, C. Foerg, H. Merkle, B. Gander, Eur. Cell Mater. 7 (2004) 11-12.

[37] J. Brugnerotto, J. Lizardi, F. Goycoolea, W. Argüelles-Monal, J. Desbrières, M. Rinaudo, Polymer 42 (2001) 3569-3580.

[38] S. Marković, Lj. Veselinović, M. Lukić, Lj. Karanović, I. Bračko, N. Ignjatović, D. Uskoković, Biomed. Mater. 6 (2011) 045005.

[39] A. Pawlak, M. Mucha, Thermochim. Acta 396 (2003) 153-166.

[40] I. Manjubala, S. Scheler, J. Bössert, K. Jandt, Acta Biomaterm 2 (2006) 75-84.

[41] Z. Gang, L. Yubao, Z. Li, L. Hong, W. Mingbo, C. Lin, W. Yuanyuan, W. Huanan, S. Pujiang, J. Mater. Sci. 42 (2007) 2591–2597.

[42] Ž. Mitić, M. Cakić, G. M. Nikolić, R. Nikolić, G. S. Nikolić, R. Pavlović, E. Santaniello, Carbohydr. Res. 346 (2011) 434-441.

[43] Ž. Mitić, G. Nikolić, M. Cakić, P. Premović, L. Ilić, J. Mol. Struct. 924-926 (2009) 264-273.

[44] R. Zhbankov, S. Firsov, D. Buslov, N. Nikonenko, M. Marchewka, H. Ratajczak, J. Mol. Struct. 614 (2002) 117-125.

[45] B. Sattelle, A. Almond, Glycobiology 21 (2011) 1651-1662.

[46] N. Nikonenko, D. Buslov, N. Sushko, R. Zhbankov, J. Mol. Struct. 752 (2005) 20-24.

[47] M. Stevanović, D. Uskoković, Curr. Nanosci. 5 (2009) 1-14.

[48] E. Fabian, R. Landsiedel, L. Ma-Hock, K. Wiench, W. Wohlleben, B. van Ravenzwaay, Arch. Toxicol. 82 (2008) 151-157.

[49] W. Phillips, B. Goins, A. Bao, Wiley Interdiscip. Rev. Nanomed. Nanobiotechnol. 1 (2009) 69-83.

[50] U. Hafeli, Radioactive microspheres for medical applications, in: M. De Cuyper, J.W.M. Bulte (Eds.), Physics and chemistry, basis of biotechnology, Kluwer Academic Publishers New York, Boston, Dordrecht, London, Moscow, 2002, pp. 213-248.

[51] D. Janković, S. Vranješ-Đurić, D. Djokić, M. Marković, B. Ajdinović, Lj. Jauković, N. Nikolić, J. Pharm. Sci. 6 (2012) 2194-2203.

[52] M. Radović, S. Vranješ-Đurić, N. Nikolić, D. Janković, G. Goya, T. Torres, P. Calatayud, I. Bruvera, R. Ibarra, V. Spasojević, B. Jančar, B. Antić, J. Mater. Chem. 22 (2012) 24017-24125.

[53] H. Mohsin, J. Fitzsimmons, T. Shelton, T.J. Hoffman, C.S. Cutler, M.R. Lewis, P.S. Athey, G. Gulyas, G.E. Kiefer, R.K. Frank, J. Simon, S.Z. Lever, S.S. Jurisson, Nucl. Med. Biol. 34 (2007) 493-502.

[54] N. Nikolić, S. Vranješ-Đurić, D. Janković, D. Đokić, M. Mirković, N. Bibić, V. Trajković, Nanotechnol. 20 (2009) 385102.

[55] Puttaswamy, A. Sukhdev, J. Shubha, J. Mol. Catal. A Chem. 310 (2009) 24-33.

[56] S. Li, L. Huang, Mol. Pharm. 5 (2008) 496–504.

[57] D. Liu, A. Mori, L. Huang, Biochim. Biophys. Acta 1104 (1992) 95–101.

[58] P. Opanasopit, M. Nishikawa, M. Hashida, Crit. Rev. Ther. Drug Carrier. Syst. 19 (2002) 191–233.

Figure captions

Figure 1. XRD analysis of HAp/Ch-PLGA, HAp/Ch, HAp, Ch and PLGA

Figure 2. FTIR spectra of HAp, Ch, PLGA, HAp/Ch and HAp/Ch-PLGA samples

Figure 3. PSD of HAp, HAp/Ch and HAp/Ch-PLGA

Figure 4. FE-SEM micrographs of: a) HAp; b) HAp/Ch and c) HAp/Ch-PLGA

Figure 5. *In vitro* stability of ^{125}I-HAp, ^{125}I-HAp/Ch and of ^{125}I-HAp/Ch-PLGA in saline and human serum during eight days. The results are expressed as the percentage of the particle-associated activity compared to the total radioactivity in medium

Figure 6. Biodistribution of a) ^{125}I-HAp (%ID/g$\pm$ S.D., n=5); b) ^{125}I-HAp/Ch (%ID/g$\pm$ S.D., n=5); c) ^{125}I-HAp/Ch-PLGA (%ID/g$\pm$ S.D., n=5)
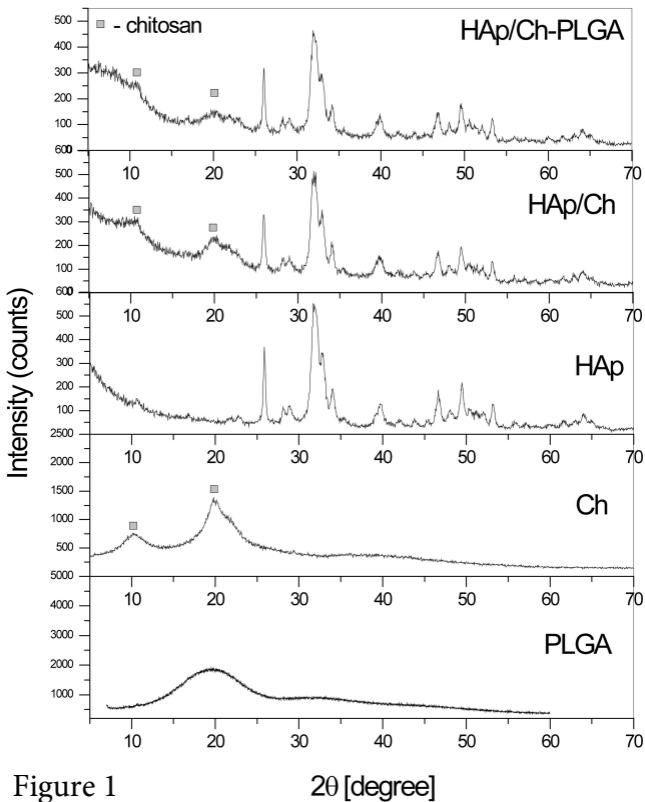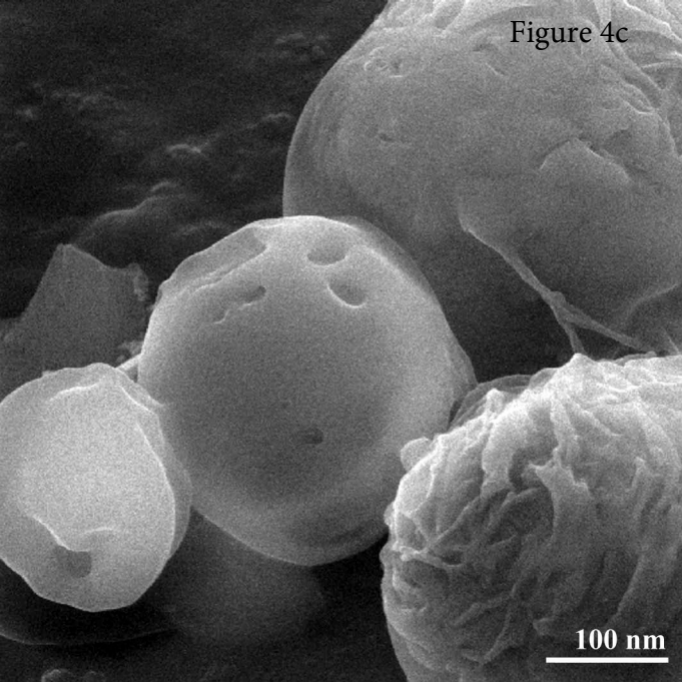
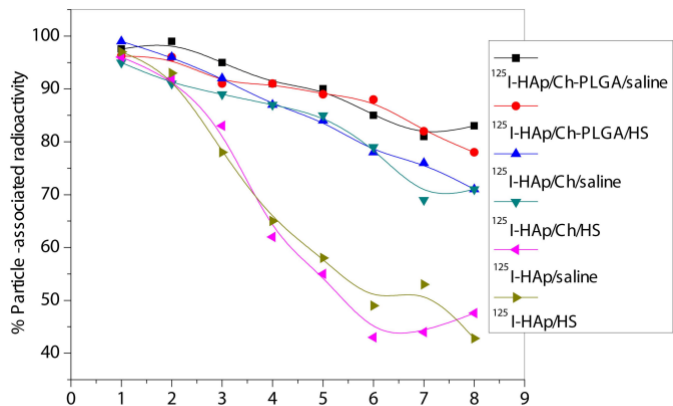Figure 1
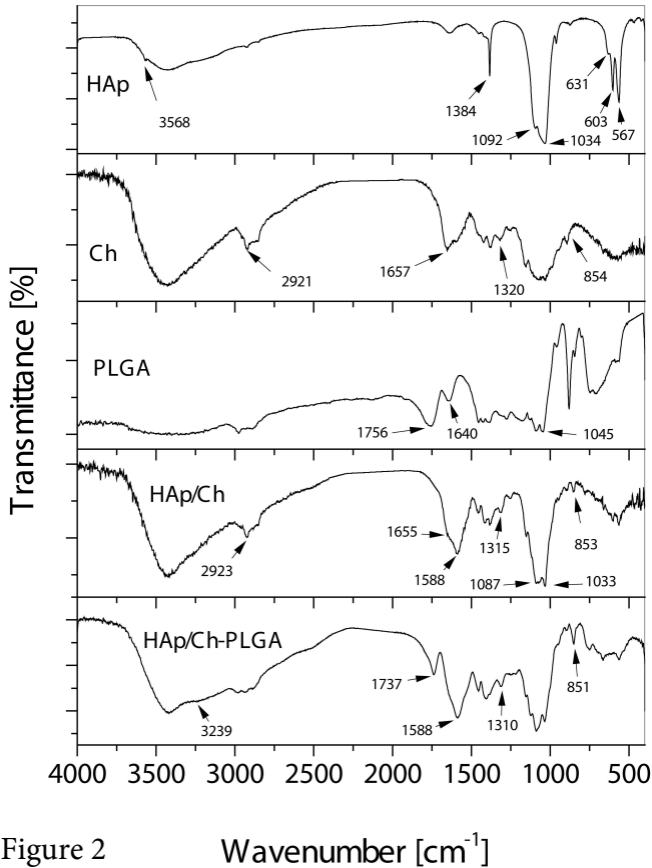
Figure 2   Wavenumber [cm⁻¹]
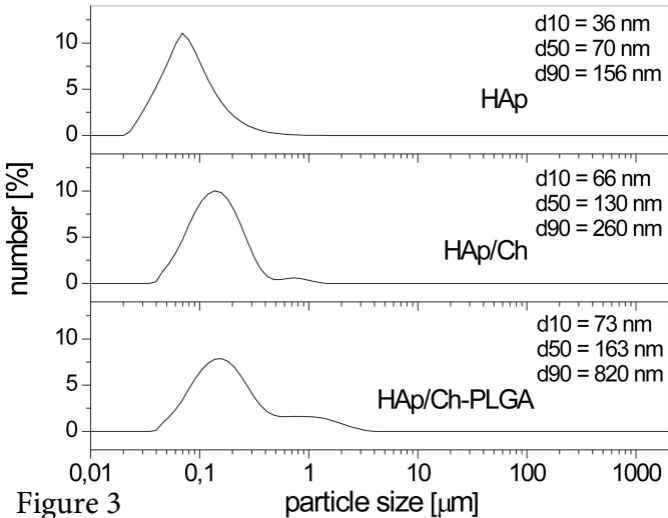
Figure 3
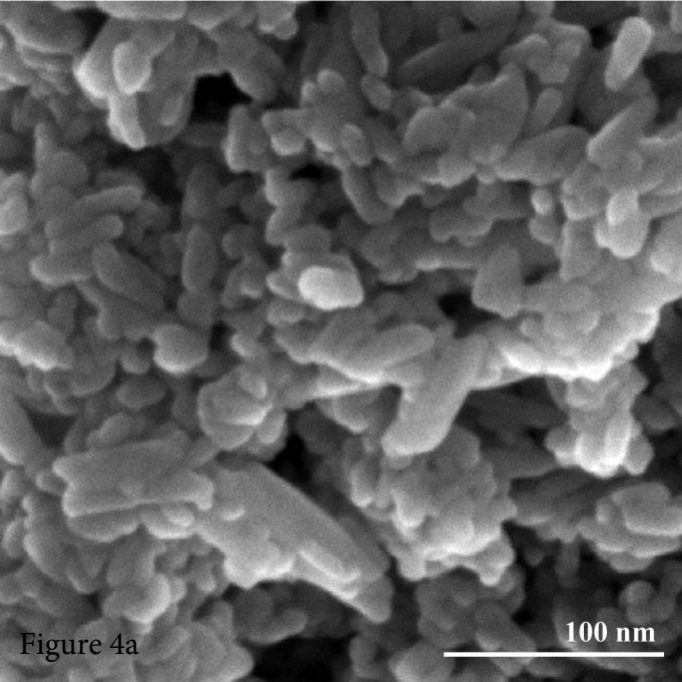
Figure 4a

100 nm

Figure 4b
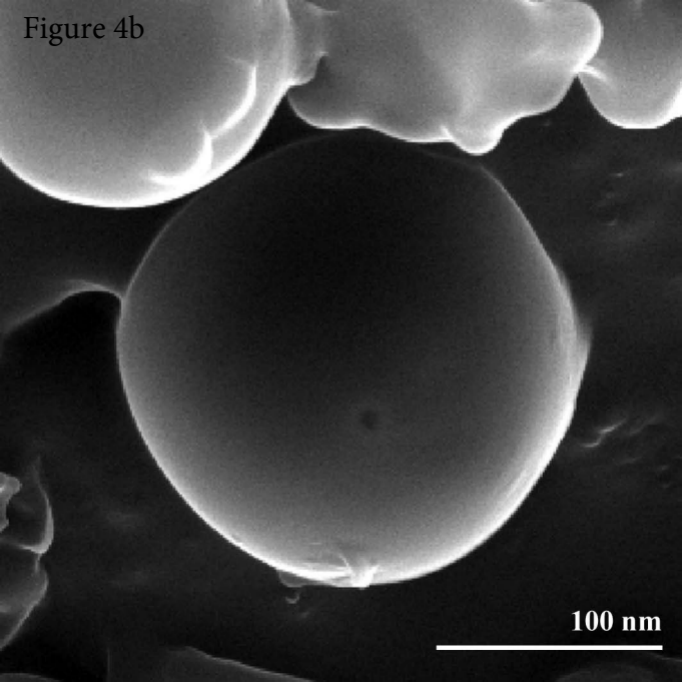
100 nm

Figure 4c

100 nm

Figure 5

Figure 6a

Figure 6b

Figure 6c